SECTION 6

SHEAR STRENGTH OF CONNECTIONS

This chapter addresses the shear strength of non-ductile slab-column connections subjected to earthquake-type loading. In older buildings, designed to resist gravity loads only, there is no protective mechanism to safeguard against collapse after the punching failure has occurred. A realistic estimation of the punching capacity of the connections is therefore essential. Based on the observed response of connection subassemblies, the punching shear strength of interior and exterior connections is determined and a procedure is suggested to calculate and relate the punching strength to the drift capacity of the connections.

6.1 Interior Connections

Among the specimens tested, only the specimens DNY_2 and DNY_4 failed in punching at interior connections. The higher intensity of the gravity load in DNY_2 and the presence of the spandrel beam in DNY_4 were the key factors that caused punching failure in these specimens. The other two specimens had flexural-yielding mechanism at the interior connections.

Moments transferred at interior connections, calculated on the basis of measured reactions were given in table 4-I. Since the specimens DNY_1 and DNY_3 did not fail in punching, the slab was able to develop its full flexural capacity, and the connections could transfer higher unbalanced moments. Axial force in the column measured as reaction at its base is shown in table 6-I.

TABLE 6-I Measured Gravity Shear at Interior Connections

Specimen	R (kips)	$\frac{V_o}{\sqrt{f_c'}b_o d}$	R/V_o
DNY_1	16.0	15.09	1.06
DNY_2	19.8	12.86	1.54
DNY_3	12.0	12.50	0.96
DNY_4	12.5	11.06	1.13

This force represents the direct shear component in the connection region. The direct shear, R, is normalized with respect to the factor $(\sqrt{f_c'}b_o d)$, where b_o is the perimeter of the critical section at a distance $d/2$ from the column face and d is the effective depth of the slab. The resulting ratios are shown in the last column of table 6-I. The specimen DNY_2 with a direct shear ratio of 1.54 had a very clear early punching failure. Specimen DNY_4 with a direct shear ratio of 1.13 was a

borderline case with shear failure occurring late in the test at about 5% drift. Observations from the test results suggest that the measured direct shear at connections can be approximated by gravity load shear, V_g, which can be easily calculated from the known gravity loads.

Initially, it is assumed that the eccentric shear stress model used in the current building code [12] can also be applied to non-ductile connections. The direct shear component can be calculated from the gravity loads as discussed earlier. The shear component generated by the unbalanced moment is determined by using the linear shear stress model. However, the effective width of the slab for moment transfer must be established first. It is to be noted that in the gravity load design of the older flat-slab buildings, the transfer of unbalanced moment is not considered and slab top reinforcement in the connection region is distributed uniformly over the width of the column strip. The observed distribution of strain in the slab reinforcement, shown in figure 4-3, suggests an effective slab width for moment transfer to be equal to the column width plus five times the slab depth $(c_2 + 5h)$. Most of the unbalanced moment at 2% drift was transferred through this slab width.

The shear strength of interior connections is estimated on the basis of shear capacity observed in specimen DNY_2 which experienced a distinct punching shear failure at the interior connection. According to the eccentric shear stress model, the shear stress is calculated by

$$v = \frac{V_u}{A_c} + \frac{\gamma_v M_{un} c_{ab}}{J_c}$$

where γ_v represents the portion of the unbalanced moment transferred through eccentric shear with the remaining unbalanced moment transferred through bending. The flexural capacity of the slab effective width of $(c_2 + 5h)$ was about 64% of the total unbalanced moment transferred at interior connection of DNY_2. The portion of the unbalanced moment transferred through shear could be taken approximately as 40%, the same as used in the present ACI building code. Accordingly, the factor γ_v is 0.4 and V_u is approximated by the gravity load shear V_g measured as column reaction R in the tests. Using the usual geometric properties as defined in the present ACI code [12], the maximum shear stress on the critical section is obtained as

$$v = \frac{19.8 \times 1000}{209.76} + \frac{0.4 \times 296 \times 1000 \times 6.9}{6784}$$
$$= 214.4 \text{ psi}$$

which expressed as a function of $\sqrt{f_c'}$ is equal to $3.5\sqrt{f_c'}$. The shear strength of the interior connection for specimen DNY_2 could therefore be taken as $3.5\sqrt{f_c'}$.

Strain distribution in slab reinforcement suggest that higher gravity loads result in narrower effective slab width for moment transfer. The effective slab width for specimen DNY_4, which carried normal service loads, was observed to be $c_2 + 7h$ compared to $(c_2 + 5h)$ as shown in figure 4-4. Furthermore, because of the lower gravity load the flexural cracking under positive bending in DNY_4 occurred adjacent to the column face, thereby reducing the effective shear area. As such, more moment is transferred through bending in DNY_4 as compared with DNY_2. The effective slab width of $c_2 + 7h$ in DNY_4 was observed to transfer 75% of the unbalanced moment with the remaining 25% transferring through eccentric shear. The γ_v factor for the case where flexural cracking under positive bending is expected to occur near the face of the column is 0.25 instead of 0.40 as discussed earlier. Based on the eccentric shear stress model, the shear strength of interior connection in DNY_4 is calculated as

$$\begin{aligned} v &= \frac{12.5 \times 1000}{209.76} + \frac{0.25 \times 390 \times 1000 \times 6.9}{6784} \\ &= 158.7 \text{ psi} \\ &= 3.0\sqrt{f_c'} \end{aligned}$$

The difference in the shear strength of the two connections, $3.0\sqrt{f_c'}$ vs. $3.5\sqrt{f_c'}$ suggests that the shear capacity of the connections is not a constant quantity but it is affected by the previous loading history including the drift level, intensity of the gravity load and yielding of the slab reinforcement in the connection region. The connections that experience large deformation reversals lose the in-plane confinement due to flexural cracking in the connection region and excessive yielding of the slab top reinforcement and hence lower shear capacity. It appears that smaller gravity loads allow larger lateral drift levels which in turn results in reduced shear capacity. The observed relationship between the shear strength factor α in $\alpha\sqrt{f'}$ and the corresponding ultimate drift is shown in figure 6-1. Based on the these results, the punching shear strength of the interior connection may be related to drift capacity by

$$\alpha = 3.8 - 0.16\Delta$$

where Δ is the inter-story drift ratio in percent. The constant 3.8 represents a conservative estimate of the punching shear capacity under pure gravity load and the shear strength factor α reduces by 0.16 for each one percent increase in the drift level.

As mentioned earlier, the deformation capacity of the connection is dependent upon the intensity of the gravity load. The observed relationship between drift and gravity shear ratio, $V_g / (\sqrt{f_c'} b_o d)$, is shown in figure 6-2. The specimen DNY_2, which was subjected to dead load

plus 100% of the live load, reached an ultimate drift of 2% with a gravity shear ratio of 1.54. The specimen DNY_4, which carried full dead load plus 30% of the live load, reached 5% drift under gravity shear ratio of 1.13. It is apparent that the intensity of the gravity load had a significant effect on the deformation capacity of interior connections. Based on the gravity shear vs. drift response of the two specimens and the previously established shear capacity under 1pure gravity load of $3.8\sqrt{f_c'}$, a relationship between the drift capacity and the applied gravity shear may be established.

Consider a 20ft. x 20 ft. floor panel with a slab thickness of 10 inches and a 20 in. x 20 in. column size. The total dead load including the self weight, floor finishes, and partitions will be of the order of 150 lbs/ft.^{2} (120 lbs/ft.^{2} for the slab and 30 lbs/ft.^{2} for floor finishes and partitions). Assuming a concrete strength of 3000 psi, the gravity shear ratio $V_g/(\sqrt{f_c'}b_0d)$ for this typical case is 1.13. This ratio in general is expected to be of the order of 1.0 to 1.2. Assuming an upper limit for drift of 7.0% corresponding to a gravity shear ratio of 1.0, a drift vs. gravity shear relationship may be obtained from the best fit (figure 6-2) through the data points(R, Δ%,...1.0, 7.0; 1.13, 5.0, 1.54, 2.0; 3.8,0) as

$$\Delta = 0.73 - \frac{6.0}{\left(\frac{V_g}{\sqrt{f_c'}b_od}\right)} + \frac{12.2}{\left(\frac{V_g}{\sqrt{f_c'}b_od}\right)^2}$$

where $V_g/(\sqrt{f_c'}b_0d)$ is the gravity shear ratio R and Δ is the lateral interstory drift in percent of the story height. Combining the $\alpha - \Delta$ and $\Delta - R$ relationships, the shear strength factor, α, may be related with the gravity shear ratio, R, by

$$\alpha = 3.68 + \frac{0.96}{R} - \frac{1.95}{R^2}$$

which is shown in figure 6-3. Conservatively, this relationship may be approximated by a straight line

$$\alpha = 2.31 + 0.39R$$

To ensure a drift capacity of at least 2% at interior connections, the gravity shear ratio must be kept less than 1.50. The calculated values of shear stress and those obtained from measured direct shear and unbalanced moments for all interior connections are given in table 6-II. The ratios of the calculated and measured shear in the case of specimens DNY_1 and DNY_3 are greater than one as these specimens did not reach their punching capacity and failed in flexural mode instead.

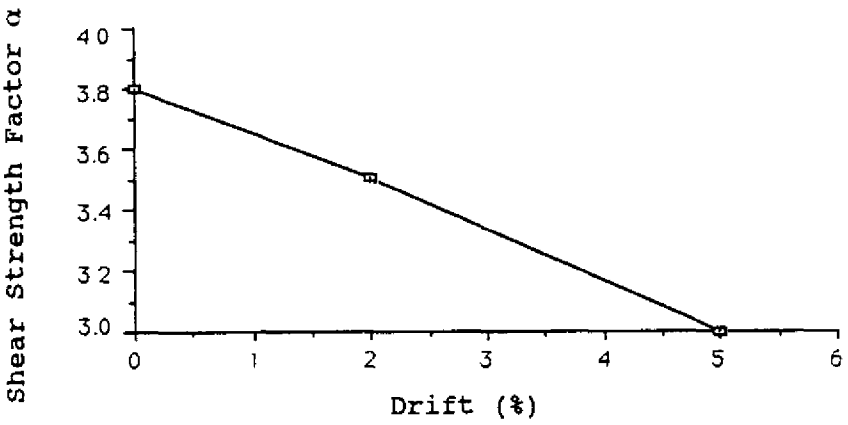

FIGURE 6-1 Shear Strength vs. Drift Relationship

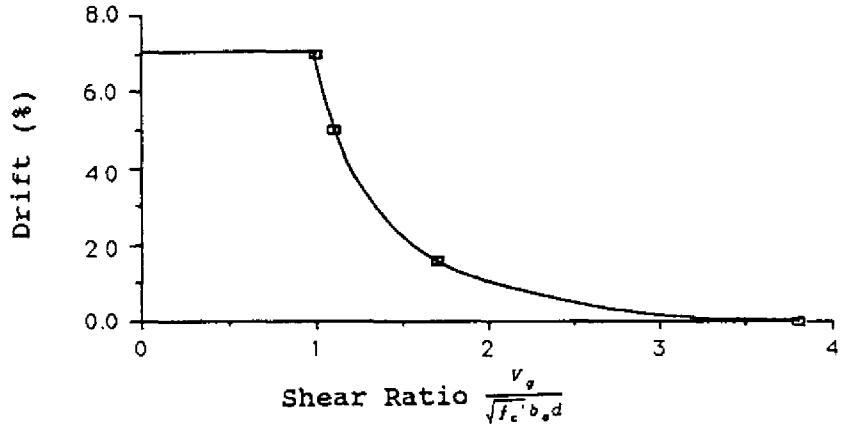

FIGURE 6-2 Gravity Shear Ratio vs. Drift Relationship

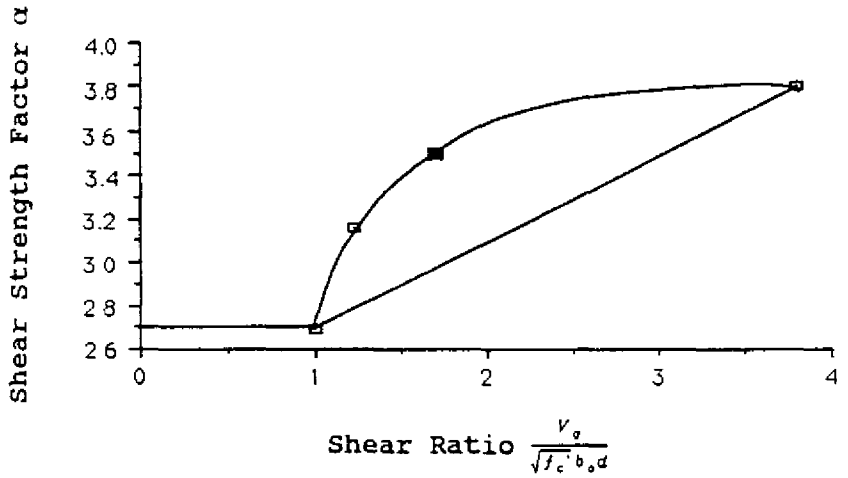

FIGURE 6-3 Shear Strength vs. Gravity Shear Ratio Relationship

TABLE 6-II Shear Strength of Interior Connections

Specimen	v_g^* (psi)	$v_{un}^\dagger$ (psi)	$v^\ddagger$ (psi)	$\alpha\sqrt{f_c'}^{**}$ (psi)	$\frac{\alpha\sqrt{f_c'}}{v}$
DNY_1	76.2	63.0	139.2	220	1.57††
DNY_2	94.4	120.0	214.4	213	0.98
DNY_3	57.1	64.6	121.7	183	1.50††
DNY_4	59.6	99.1	158.7	154	0.97

*. shear stress due to gravity load
†. shear stress due to unbalanced moment
‡. total shear stress
**. calculated shear strength
††. connection did not reach its punching capacity

6.2 Exterior Connections

The behavior of exterior connections was typically characterized by a combination of bending and torsional action as observed ina number of previous studies (Robertson and Durrani, 1990). The exterior connections lost their stiffness quite rapidly, hence the punching shear failure under lateral load never materialized. The shear acting on the critical section of the exterior connection, measured as column reaction during the test, includes shear resulting both from gravity and lateral loads. The gravity load shear did not change much during the test from that measured at the initial condition under pure gravity load. The increase in shear, therefore, resulted mostly from the lateral load. The variation of total shear with drift is shown in figure 6-4 where the shear is normalized with respect to $\sqrt{f_c'}b_o d$, where b_o is perimeter of the critical section assumed at a distance d/2 from the column face. The gravity shear ratio at the initial condition varied between 0.6 and 0.9 which is represented by the first point on the curve at zero drift.

The specimen DNY_2 which resisted heavier gravity load is of particular interest since it experienced punching failure at the interior connection. The shear under lateral load increased by 50% at 2% drift when the interior connection failed in punching shear. At this drift level, the shear stress at the exterior connection was $1.3\sqrt{f_c'}$ which is relatively low to cause a punching failure.

The increase in shear due to lateral load in the other three specimens was relatively smaller. As exterior connections developed the flexural-torsional mechanism, the load redistributed to interior connections and the net shear at the exterior connection and the net shear at the exterior connec-

tions remained low. Since none of the exterior connections failed in punching, the punching shear strength of the exterior connections could not be determined. However, it is clear that if the gravity load shear is limited to $0.8\sqrt{f_c'}b_o d$, at least 3.5% lateral drift can be achieved without a punching failure. Similarly, if the gravity shear is $0.9\sqrt{f_c'}b_o d$, a drift of at least 2% is achievable.

The observed shear and moment at the exterior connections is shown in figure 6-5. The shear is normalized with respect to $\sqrt{f_c'}b_o d$ and the moment is normalized with respect to M_o which is the flexural capacity of the exterior connection as defined in Chapter 5. The relationship between shear and moment appears to follow a similar trend in all specimens. In each case, the moment increased faster than the shear did. The difference in the initial shear and moment of the specimens are due to different gravity loads and different initial stiffness. The specimen DNY_4 with a spandrel beam carried more initial shear due to higher stiffness at the exterior connection and the specimen DNY_2 had higher initial shear and moment due to larger gravity load. Since none of the exterior connections failed in shear, the moment transfer was affected mostly by the rate of stiffness degradation. The specimen DNY_2 did not reach its moment capacity because of the early punching failure at the interior connection. Once the interior connection punched, the load redistributed to the exterior connection and the shear increased rapidly. However, in none of the specimens, the shear could reach high enough level to cause a punching failure. The net shear due to gravity load and moment transfer reached a maximum of $1.3\sqrt{f_c'}b_o d$ in specimen DNY_2 which had the highest gravity load. It can therefore be concluded that, for initial gravity shear at exterior connections of $0.9\sqrt{f_c'}b_o d$ or less, the response is governed primarily by bending and torsion of the slab edge.

Under positive bending, the net shear on the critical section is reduced due to the opposing effects of gravity shear and the lateral load. Also, the net moment at the column face depends on the relative magnitude of the gravity load and the lateral load moments. As observed during the testing of specimens, the possibility of a failure under net positive moment at the column face is relatively small. Even if the slab cracked in positive bending, the net shear area is sufficient to resist the low shear at exterior connections.

6.3 Analytical Model For Connection Strength

The discussion of connection strength in the previous section was based on the linear shear stress model specified in the current ACI Building Code and the allowable shear stress and moment-transfer factors were suggested to reflect the non-ductile detail of the slab-column connections. Attempt is made in this section to further modify the linear shear stress model to more realistically represent the unsymmetrical cracking pattern at the interior connection by changing the effective shear area of the critical section.

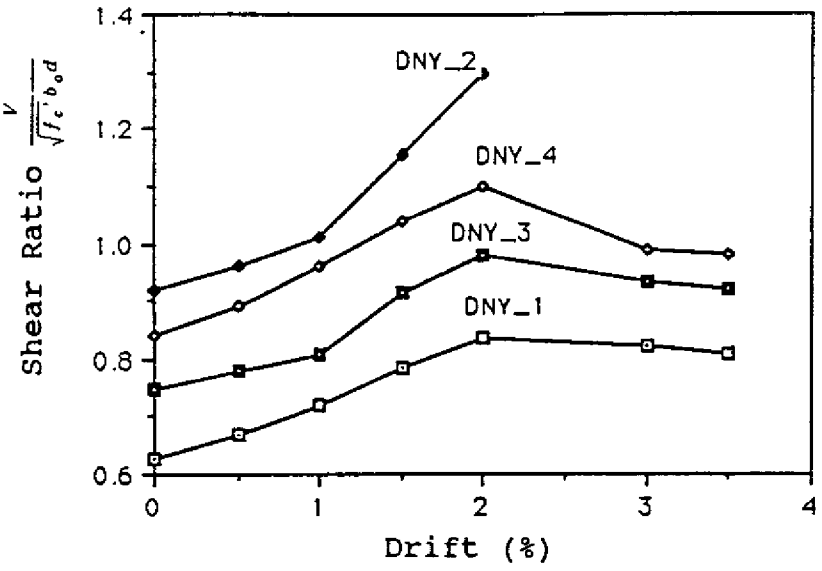

FIGURE 6-4 Measured Shear Force Variation With Drift at Exterior Connections

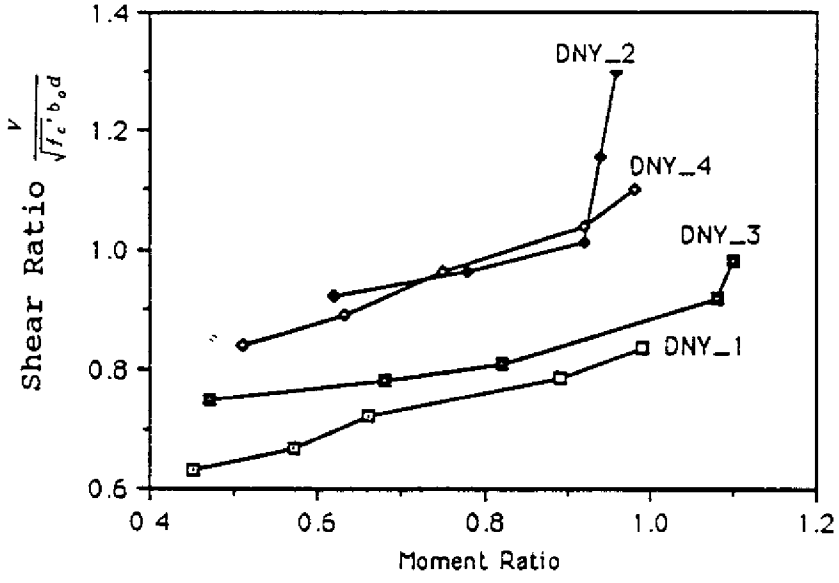

FIGURE 6-5 Measured Shear Force With Unbalanced Moment at Exterior Connections

6.3.1 Interior Connections

Test results have shown that the moment transfer at connections occurred primarily on the column face subjected to negative moment with slab top reinforcement in tension. On the opposite face of the column, the slab under positive moment had at best a moment transfer capacity equal to the cracking strength of the slab. Depending on the intensity of the gravity load, the flexural cracks under positive bending were observed to occur between 0.25d and d distance away from the face of the column, where d is the slab effective depth. The presence of such a crack reduces the net area available for shear resistance on that face. Consequently, most of the shear and moment at interior connection is transferred mostly through the remaining three faces of the slab critical section. The eccentric shear stress model for connections could therefore be modified to reflect this behavior of non-ductile slab-column connections.

In order to simplify the shear model, it is assumed that (i) the flexural crack on the bottom of the slab is located at a distance d/2 from the column face, and (ii) the shear and bending capacity of the cracked slab under positive bending is negligible. The modified slab critical section, shown in figure 6-6, may be considered as fixed on three faces and hinged on the face with slab under positive moment. A finite element analysis of plate with such boundary conditions and subjected to gravity load and moment at the center indicates that only 8% of the direct shear and 7% of the shear from the moment is transferred through the hinged edge. Conservatively, the shear and moment transfer at the cracked slab edge subjected to positive bending may be ignored. The net effective critical section for shear stress calculations may therefore be assumed to consist of three sides as illustrated in figure 6-6. The eccentric shear stress model can then be applied to this critical section to determine the maximum shear stress in the connection region.

As described previously, the effective width for unbalanced moment--transfer is taken as $c_1 + 5h$, with 25% of the unbalanced moment being transferred through eccentric shear. The geometric properties of such a critical section are very similar to that of the exterior connections used in the ACI Building Code (11). The area of the critical section is

$$A_c = d\,[2\,(c_1 + d) + (c_2 + d)\,]$$

and

$$J_c = \frac{2da^3}{3} - (2a + b)\,dx_1^2 + \frac{ad^3}{6}$$

where $a = c_1 + d$ and $b = c_2 + d$, and x_1 is the distance from centroid of the critical section to the inside face of the critical section.

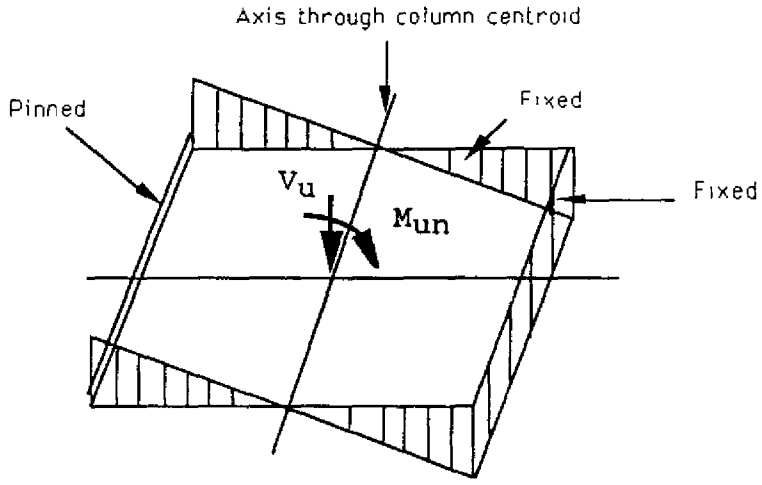

FIGURE 6-6 Shear Stress Distribution With Hinge Support on One Side of Critical Sections

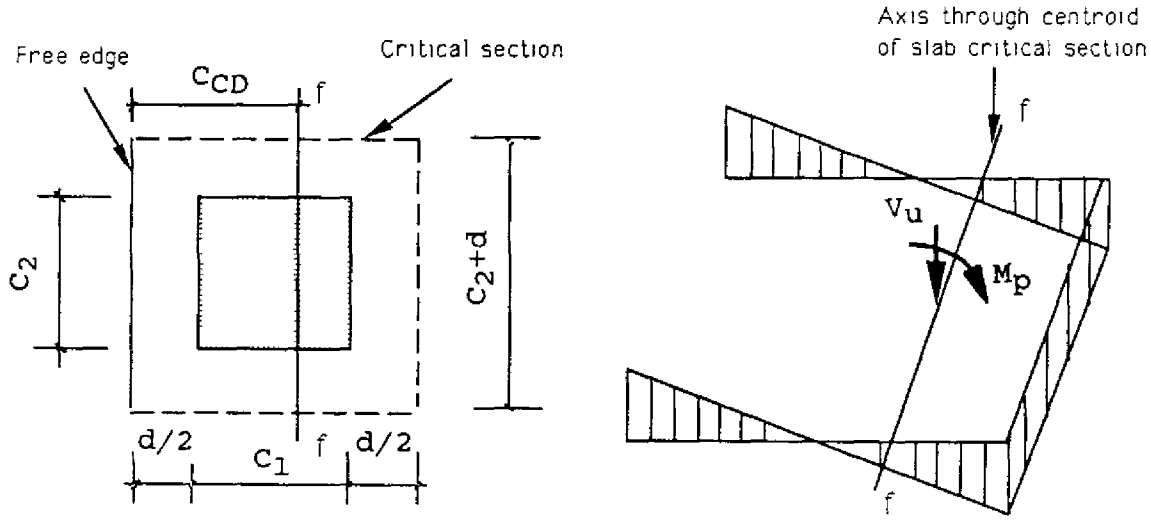

FIGURE 6-7 Proposed Critical Section for Shear at Interior Connections

The shear stress can then be calculated in a usual manner by

$$v = \frac{V_u}{A_c} + \frac{\gamma_v M_{un} c}{J_c}$$

The shear stress values calculated by this procedure are compared with the measured values in table 6-III. The calculated values using the modified critical section appear to agree well with the values based on the test results.

TABLE 6-III Shear Strength by Modified Linear Shear Stress Model

Specimen	v_g (psi)	v_{un} (psi)	v (psi)	$\alpha\sqrt{f'_c}$ psi	$\frac{\alpha\sqrt{f'_c}}{v}$
DNY_1	101.7	105.1	206.8	243	1.18
DNY_3	76.2	108.1	184.3	192	1.04
DNY_4	79.5	98.5	178.0	180	1.01

6.3.2 Exterior Connections

Since none of the exterior connections failed in punching, the shear strength of exterior connections could not be determined on the basis of test results. Based on the test observations, the likelihood of a punching failure occurring at the exterior connections appears to be relatively small. The response of the exterior connections was typically controlled by a combination of bending plus torsion of the slab edge. The unbalanced moment-transfer capacity of the exterior connections is therefore a combination of the flexural strength of a certain width of the slab and the torsional strength of the slab edge. The width of the slab used in calculating the flexural strength depends upon the stiffness of the slab edge. For the exterior connection without an edge beam, the unbalanced moment transfer capacity may be calculated by

$$M_{un} = M_{c1+c2} + 2M_t$$

where M_{c1+c2} is the flexural strength of the slab over the width $c_1 + c_2$ centered on the column line and M_t is the torsional strength of the slab edge. However, when a spandrel beam is present, the moment transfer mechanism depends upon the relative strength of the slab in flexure and the torsional strength of the slab edge. For the case where the slab has a strong edge beam, the moment-transfer mechanism is in the form of a yield line across the full width of the slab and the full flexural capacity of the slab is mobilized under lateral load.

SECTION 7

CONCLUSIONS

7.1 Summary

An experimental investigation was conducted to evaluate the seismic resistance of slab-column connections in flat-plate buildings which are designed and detailed to resist gravity loads only. The study focused on buildings constructed during the fifties and sixties. Four two-bay flat-plate subassemblies were designed and detailed following the design procedures in building codes of that period and tested under earthquake type loading. Based on the observed response of the subassemblies and individual connections, conclusions are drawn on strength, stiffness, and deformation capacity of the subassemblies, interior connections, and exterior connections.

7.2 Subassembly Response

(1) Lateral load resistance of the two-bay slab-column subassembly depended on the failure mode of connections. Under high gravity loads, punching dominated the response and the lateral resistance of the subassembly was limited by the punching strength of the interior connection. Under normal service loads, flexural yielding of the slab dominated the response and the lateral resistance was limited mainly by the flexural strength of the slab under negative bending. The contribution of the slab under positive bending at connections was limited to its cracking strength and became negligible after the slab reached its cracking capacity.

(2) The presence of a spandrel beam increased the initial lateral stiffness and an increase in the gravity load reduced the initial stiffness. Approximately 70% of the initial stiffness was lost during the first 2% lateral drift. Beyond this drift level, the stiffness of the subassemblies degraded in a similar manner and was independent of the specimen configuration.

(3) The intensity of the gravity load on the slab had the most effect on the lateral drift capacity of the subassembly. Under normal service load condition (DL+0.3LL), the subassemblies were able to reach a lateral drift of at least 4.5%. At full dead and live load, the lateral drift capacity reduced to 2%. The presence of an edge beam and the bent-up reinforcing detail in the slab both appear to improve the ductility of the slab-column subassemblies.

(4) Under normal service load conditions, the lateral load is resisted primarily by a flexural yielding mechanism with yield lines developing across the full width of the slab at the interior connections and a flexural-torsional mechanism of the slab edge at the exterior connections. Because of the low

reinforcement ratio in the slab, the load-deformation response of the subassemblies is approximately bilinear.

(5) The lack of adequate anchorage or failure of anchorage of the slab bottom reinforcement in the connection region did not have any obvious effect on the overall lateral resistance of the subassemblies. However, in the event of a punching failure at the interior connection, the slab top reinforcement was not able to sustain the gravity load on the slab.

(6) The share of the lateral load carried by the interior column increased as the stiffness of the exterior connections degraded. Under full dead and live load action, approximately 60% of the lateral load was carried by the interior column at 2% drift.

7.3 Interior Connections

(1) The mode of failure of non-ductile interior slab-column connections under seismic loading depends largely on the level of gravity shear applied to the connection. For a gravity shear ratio, $V_g / (\sqrt{f_c'} b_o d)$, of 1.0 or less, the mode of failure was primarily flexural. However, with a gravity shear ratio of 1.5, the mode of failure changed to that of punching shear.

(2) The punching shear capacity of the connection decreased with the increasing drift level and yielding of the slab reinforcement. Based on the eccentric shear stress model of the ACI Building Code, the shear strength of the interior connection varied between $3.5\sqrt{f_c'}$ at 2% drift to $3.0\sqrt{f_c'}$ at 4.7% drift.

(3) The unbalanced moment transfer at connection occurred mainly through negative bending of the slab. Under positive bending, the moment transfer was limited to cracking strength of the slab. With non-ductile reinforcing detail, the negative flexural strength of the column strip gave the best estimate of the unbalanced moment-transfer capacity of the interior connection.

(4) The connection stiffness degraded rapidly losing 75 to 85% of the initial stiffness by 2% lateral drift. Provided the gravity load is small and the punching failure does not occur, the connection is able to sustain at least 80% of the lateral load through at least 4% drift though at a considerable loss of stiffness.

(5) A modification of the critical section used in the eccentric shear stress model is proposed. This model accounts for the observed limited capacity in shear and moment transfer between the column and the slab under positive bending after the slab has reached its cracking capacity. The suggested three-sided critical section appears to better predict the shear strength of the interior connections.

7.4 Exterior Connections

(1) None of the exterior connections failed in punching shear. The limited torsional capacity of the slab edge acted more like a fuse and transferred the load to the interior connection, thus protecting the exterior connection from a punching failure. The exterior connections were able to sustain a gravity shear ratio ($V_g / (\sqrt{f_c'} b_o d)$ of 0.75 through 4-5% drift without a punching failure. This however did not represent the maximum shear capacity as none of the connections reached their punching strength.

(2) The unbalanced moment-transfer under negative bending at exterior connection is limited to $M_{c1+c2} + 2T_c$, where M_{c1+c2} is the flexural capacity of the slab width $c1 + c2$ centered on the column line and T_c is the cracking torsional strength of the slab edge. If a strong edge beam is present, the connection is able to develop flexural strength of the entire width of the slab. In the positive moment direction, the moment transfer is limited to cracking strength of the slab.

(3) The exterior connection lost their stiffness much faster than the interior connections losing approximately 70 to 75% of the initial stiffness in the negative moment direction by 1% drift. In the positive moment direction, the stiffness became negligible after the slab reached its cracking strength.

(4) The slab bottom reinforcement extending into the exterior connection yielded as soon as the slab reached its cracking moment. Under repeated load reversals, the anchorage of slab bottom reinforcement was completely lost by about 2.25% lateral drift.

SECTION 8

REFERENCES

1. "Impressions of the Guerrero-Michoacan Mexico Earthquake 19, September, 1985," A Preliminary Reconnaissance Report, EERI, October 1985.
2. "CSMIP Strong-Motion Records from the Whittier, California Earthquake of 1 October, 1987," California Department of Conservation, Division of Mines and Geology, Report OSMS 87-05.
3. "Building Regulations for Reinforced Concrete ACI 318-41," American Concrete Institute, Detroit, 1941.
4. "Building Regulations for Reinforced Concrete ACI 318-47," American Concrete Institute, Detroit, 1947.
5. "Building Code Requirements for Reinforced Concrete ACI 318-51," American Concrete Institute, Detroit, 1951.
6. "Building Code Requirements for Reinforced Concrete ACI 318-56," American Concrete Institute, Detroit, 1956.
7. "Building Code Requirements for Reinforced Concrete ACI 318-63," American Concrete Institute, Detroit, 1963.
8. "The Shear Strength of Reinforced Concrete Members-Slabs," ASCE-ACI Task Committee 426 ASCE Journal of Structural Division Vol.100. No.ST8. August 1974, pp. 1543-1591.
9. "Building Code Requirements for Reinforced Concrete ACI 318-89," American Concrete Institute, Detroit, 1989.
10. "Recommendations for design of Slab-Column Connections in Monolithic Reinforced Concrete Structures," ACI Committee 352, 1989, p. 22.
11. Vecchio, F. and Collins, M., "Investigating the Collapse of a Warehouse" ACI Concrete International, March 1990, pp 73-78.
12. Hsu, T, "Torsion of Reinforced Concrete," John Wiley, 1984, p.516.
13. Cope, R. and Clark, L., "Concrete Slabs Analysis and Design," Harper and Row, 1984, p. 502.
14. Wang, C.and Salmon, C., "Reinforced Concrete Design," Harper & Row, Fourth Edition, 1985, p. 947.
15. Park, R.and Paulay, T., "Reinforced Concrete Structures," Wiley-Interscience, 1975. p. 769.
16. Victor, D., "Reinforced Concrete T-Beams Without Stirrups Under Combined Moment and Torsion," Journal ACI Vol 65 No.1 Jan. 1968. pp 29-36.
17. Robertson, I. and Durrani, A., "Seismic Response of Connections in Indeterminate Flat-slab Subassemblies," Structural Research at Rice Report No.41, July, 1990, p. 266.